NASA TN D-1148

TECHNICAL NOTE

D-1148

A CORRELATION STUDY OF THE BOW-WAVE PROFILES OF BLUNT BODIES

By Alvin Seiff and Ellis E. Whiting

Ames Research Center
Moffett Field, Calif.

NATIONAL AERONAUTICS AND SPACE ADMINISTRATION

WASHINGTON

February 1962

NATIONAL AERONAUTICS AND SPACE ADMINISTRATION

TECHNICAL NOTE D-1148

A CORRELATION STUDY OF THE BOW-WAVE PROFILES OF BLUNT BODIES

By Alvin Seiff and Ellis E. Whiting

SUMMARY

A study was made of experimental bow waves and bow waves calculated by numerical integration of the flow equations, for blunt-nosed bodies of revolution. The purpose was to obtain a systematic description of the bow-wave profiles and to find how they varied with nose shape, Mach number, and total enthalpy. Emphasis was placed on the nose region as well as on the downstream region of the waves. The method of approach was to fit equations of the form suggested by blast-wave theory to the bow-wave profile data, and to seek correlations of the constants in the equations. The study included seven blunt-nosed shapes, Mach numbers from 3.5 to 19.3, and corresponding total enthalpies from 400 to 8100 Btu/lb.

The power-law equation, which is the generalized form of the blast-wave theoretical equation, could in all cases give a good representation of the bow-wave profiles. In one case - the hemispherical nose - a single equation describes the wave over the entire surface from the axis to the downstream station where the Mach angle limitation begins to affect the profile. In general, however, two or more sets of coefficients in the equation are required to describe the complete wave. For bodies blunter than the hemisphere, for example, two equations are needed - one for the nose region and one for the downstream region.

The coefficients in the equation vary systematically with Mach number or with total enthalpy for any given configuration, but correlate better with the total enthalpy. In the case of the power-law exponents for the downstream wave regions, a single curve gives a good approximation to the variation with total enthalpy for four of the seven bodies investigated, the hemisphere and the three blunter shapes. It was also found that the constant of proportionality in the equation varies with the fourth root of the drag coefficient, a result given by blast-wave theory. For the very blunt shapes, the exponent in the nose region is lower than in the downstream region. The ratio of these exponents is nearly a fixed fraction for any given nose shape, and depends on the nose fineness ratio.

INTRODUCTION

Bow-wave profiles of blunt-nosed bodies of revolution in hypersonic flow are of interest from the standpoint of obtaining a quantitative description of the flow disturbance surrounding the body in flight. Such a description can have many applications. In reference 1, for example, a procedure is given by which the bow-wave profile may be used to obtain the detailed structure of the downstream regions of the disturbed flow field. This kind of information would in turn be required to determine the heat transfer to a cylindrical afterbody, the interference effect of the body flow field on other vehicle components, or the degree of ionization of the stream enveloping the cylinder, and so forth.

The shape of the bow wave of a blunt-nosed body is predicted by Lin's theory of cylindrical blast waves (ref. 2) to be a paraboloid, with the radius of cross section at any given station depending on the one-fourth root of the drag coefficient. This implies that the wave shape is nearly independent of the shape of the blunt nose; that is, all blunt-nosed bodies generate approximately the same bow wave. This is perhaps a good generalization for very rough purposes.

One of the first reports to compare experimental bow waves with Lin's equation was reference 3, where it was noted that for helium flow around a hemisphere cylinder the form of the equation is correct, but the coefficients have to be adjusted to fit the observed bow wave. Inasmuch as helium has a different value of the ratio of specific heats, γ, from that assumed by Lin, it was of interest to find that this conclusion holds for air also, as noted in reference 4; that is, the coefficients in the equation must be adjusted for air flow, as well as for helium flow. The adjusted equation gives a very good fit to a large region of the wave.

Van Hise, in reference 5, added to this picture by correlating the bow-wave profiles from a number of characteristic solutions for pointed bodies in perfect air ($\gamma = 1.4$) at very high Mach numbers. He was able to correlate the waves of all these bodies, for the region beginning a few diameters downstream of the body apex, by use of an equation of the form suggested by Lin, but again with adjusted coefficients. For example, the power of x (downstream distance from wave apex) in Van Hise's correlation is 0.46 instead of 0.50.

The present investigation began when the authors found that they had need for bow-wave profile information which could not be satisfied by the previously published information. The published information is deficient primarily in that it is not applicable to the nose region, which is usually the region of greatest interest. Other limitations are that no systematic body of information is available for blunt-nosed configurations, and that much of the available information is for constant ratios of specific heats of 1.4 and 1.67, in contrast to real air flows in which the ratio of

specific heats is variable and usually smaller than 1.4. The present paper will not definitively fill the need for this extended information, but will be aimed at contributing toward it.

Specifically, the bow-wave profiles of a number of blunt-nosed bodies were measured and studied for both the nose regions and the downstream regions of the waves. The waves were fitted by equations of the form suggested by the blast-wave theory, and an effort was made to correlate the coefficients in the equations in terms of nose shape, Mach number, and total enthalpy. The shadowgraphs came from previously completed test programs in the Ames Supersonic Free-Flight Wind Tunnel (refs. 6 through 10). The data cover the Mach number range from 3.5 to 16 with a corresponding range of total enthalpies from about 400 to 2400 Btu/lb.

SYMBOLS

a	coefficient in equation (4)
C_D	nose pressure drag coefficient, dimensionless
d	cylinder diameter, ft
d_t	diameter of spherical tip, ft
h_s	total enthalpy, Btu/lb
k	coefficient in equation describing bow-wave profile, dimensionless
$\left(\frac{l}{d}\right)_n$	nose fineness ratio
M_∞	free-stream Mach number
m	exponent in equation (4)
n	exponent in equation describing bow-wave profile, dimensionless
r_s	radius of cross section of shock wave, ft
R	nose radius of curvature, ft
x	coordinate along body axis, zero at wave apex, ft
γ	ratio of specific heats
μ	Mach angle, deg
θ	cone half-angle, deg

Subscripts

D downstream

hs hemisphere

PRESENTATION OF DATA

Method of Analysis

Lin's equation for the bow-wave profile is

$$r_s/d = 0.80\ C_D^{1/4}(x/d)^{1/2} \qquad (1)$$

The more general equation which is found in references 3 through 5 to fit certain regions of experimental and exact theoretical bow waves is

$$r_s/d = k(x/d)^n \qquad (2)$$

Equations of this form plot as straight lines on logarithmic plotting paper. Hence, a convenient way to test the applicability of equation (2) to a given experimental shock wave is to plot its coordinates on logarithmic paper. If the plot is straight in any region, equation (2) applies in that region, and k and n can be evaluated. This is the procedure which was applied to the present data.

Results obtained will be discussed in three sections: Hemispheres, Noses Blunter Than Hemispheres, and Round-Nosed Cones. The configurations studied are shown in figure 1. Although not shown in the figure, the afterbody configurations varied; for example, some of the noses were tested without an afterbody. These variations are not believed to have importantly affected the results obtained, since when the afterbody was missing, the measurements were limited to 2 or 3 diameters downstream of the nose.

Hemispherical Noses

Logarithmic plots of the shock waves from two hemispherical noses are given in figure 2. Substantial regions of these plots can be very well fitted by straight lines. The fitted equations are given in the figures. It can be seen that these equations describe the wave into the nose region, up to about $x/d = 0.1$ in figure 2(b).

A total of 11 hemisphere and hemisphere-cylinder shadowgraphs were treated in this way and the results are summarized in table I. Four shock

waves from theoretical solutions are also included in the table and will be discussed later in the report. The constants listed as k_2 and n_2 are coefficients appropriate to the main body of the wave. In cases where a better fit to the nose region of the wave ($x/d < 0.3$) could be obtained by a second straight line, coefficients designated k_1 and n_1 are listed. It is problematical for the case of the hemispherical nose whether these deviations in the nose region are real or are due to measurement errors which are maximum in the nose region. These deviations will be further considered under Discussion.

Far downstream, the wave angle must approach the Mach angle and remain nearly constant. Then the equation of the wave becomes

$$\frac{r_s}{x - x_o} = \tan \mu \tag{3}$$

where x_o is the intercept of the asymptote on the axis of symmetry. On logarithmic paper, for $x \gg x_o$, equation (3) describes a straight line of unit slope. Hence the profile data can be expected to approach unit slope in the far downstream region. A tendency to turn toward this limit is apparent in figure 2(a) at $x/d > 10$. This region of the wave was not of primary interest to the authors and will not be discussed.

Noses Blunter Than Hemispheres

Figure 3 shows logarithmic plots of the bow waves of a flat-faced circular cylinder, a convex spherical-segment face, and a 1/7-power nose, all at Mach numbers slightly above 1.4. In these cases, very plainly, a single straight line will not fit the data for the nose region and the downstream region. However, two straight lines will come very close to giving the ordinates of the wave at all stations from x/d of 0.1 to 10. At the intersection of the two straight lines, a discontinuity in wave angle is implied by this representation, which is clearly unrealistic. When wave angle is desired, suitable smoothing of the intersection is required.

A physical interpretation of the change in line slope is as follows: In the forward region, the wave radius of cross section is forced into rapid growth by the rapid growth in cross section of the blunt nose. The exponent n assumes values as low as 0.3. If the exponent were to be reduced to zero, the wave would become a step wave and hence would match the contour of the flat-faced cylinder. In the downstream region, a growth rate closer to that predicted by blast-wave theory is permissible.

Values of the coefficients k and n are given in table I for the three noses blunter than hemispheres, for both the nose region and the downstream region. The points of intersection of the two regions can easily be determined by solving their defining equations simultaneously.

Round-Nosed Cones

In figure 4, the logarithmic plot of two wave profiles from round-nosed cones shows them to be more complicated than the other cases. However, remarkably enough, the waves can now be represented by three straight-line segments. The nose region line is the one that would be expected to be generated by the spherical tip (see lines marked "expected sphere wave," fig. 4). A transition section occurs beginning where the conical part of the body predominates in defining the wave profile. A far downstream section then begins, and it is the latter section that would be expected to agree most closely with blast-wave theory. A shadowgraph picture is presented in figure 5 marked to show the intersections of the three line segments. Data collected on round-nosed cones are given at the end of table I.

DISCUSSION AND CORRELATION

The data presented above are evidently very complicated. Certainly, in the region near the nose, special rules will be needed for each class of body. In addition to the nose shape, other significant variables include the flow Mach number and total enthalpy. The latter would be expected to influence the wave shape primarily through its effect on the ratio of specific heats. An effort will now be made to systematize this information, insofar as possible, beginning with the hemispherical nose.

Hemispherical Nose

The data collected in table I on the coefficient k and the exponent n for $x/d > 0.3$ are plotted against Mach number in figure 6. The variation is systematic with relatively small scatter. As noted in the legend, the square symbols represent cases in which the maximum rearward extent of the data was to $x/d < 2$. These cases always fell slightly below the curves faired through the data which extended farther downstream. If the presentation is limited to the open circular data points, the scatter is very small indeed.

The filled and half-filled data points were obtained from the theoretical solutions for the flow about hemisphere cylinders. The three filled symbols were obtained from solutions privately communicated by the General Electric Company; these were calculated by the method of reference 11. The half-filled symbol was obtained from data given in reference 12. These results are close to the curve through the present experimental values. It was suspected that the remaining disagreement might be partly due to large differences in total enthalpy between these results and the experimental results (see table I). A plot of the circular data points was therefore made with total enthalpy as the independent

variable. The results are shown in figure 7. Here, the solid points can be smoothly connected with the present data, but the half-filled point still cannot be brought precisely into line unless the variation of the exponent n with enthalpy is permitted to show a minimum at about 2000 Btu/lb.

The total enthalpy is a measure of the speed and hence of the degree of dissociation, and excitation in the disturbed gas layer. However, the equilibrium composition of the gas also depends, to a lesser extent, on the density level in the disturbed flow field and hence in the free stream. Thus, it is to be doubted that one curve would correlate all possible combinations of speed and altitude, particularly if the variations in ratio of specific heats in the downstream flow field play a measurable part in determining the wave profile. This may be the explanation of the imperfect correlation of the data point from reference 12 which was for the case of a high speed and a low altitude. Figure 7, in this view, would be thought of as one member of a closely spaced family of curves, representing different flight altitudes. However, it should be admitted that the failure of the one point to correlate may also be due to some inaccuracy in the theoretical solution.

The nose-region constants from table I are plotted against Mach number in figure 8. The upper two sections of the figure show these data compared with the curves of figure 6. It can be seen that the scatter is rather appreciable, but that the nose-region data may lie a little above the downstream curves. The lower part of the figure shows the station of transition from nose region to downstream coefficients. The trend is for this station to move rearward with increasing Mach number. For many purposes, these deviations in the nose region of the wave profile could be neglected in the case of the hemispherical blunt nose.

Noses Blunter Than Hemispheres

Downstream region.- A presentation of the downstream wave coefficients in terms of Mach number is shown in figure 9 for the three noses blunter than the hemisphere. The hemisphere curves from figure 6 are also reproduced. As with the hemisphere, these data show regular variation with small scatter. Note that only one data point is presented for the convex circular-arc blunt nose.

The variation of the coefficient k with Mach number, in the case of the 1/7-power nose, is not very similar to those for the hemisphere and the flat nose. This is believed to be due to the nearly constant value of total enthalpy which was maintained for this model over the Mach number range from 7.7 to 14.5 (see ref. 7). As a result, the relation between total enthalpy and Mach number for this configuration is not the same as for the other two bodies with which it is compared. In figure 10, the data are plotted against total enthalpy, with the hemisphere data brought forward from figure 7 (circular symbols). An improved comparison

is obtained. In fact, for the exponent n, one curve can be used to represent all the test bodies. In a certain region, the data for the flat-faced body fall below this curve, but only by about 1 or 2 parts in 50. The improved correlation compared to figure 9 indicates that, at hypersonic speeds, the total enthalpy is more important than the Mach number in defining the wave profile.

The flagged point, which has been included for completeness, disagrees with the other data for an apparent reason. This point is for a low test Mach number, 4.5, for which the approach to the Mach angle begins at very low x/d. If the data in this case are restricted to $x/d < 4$, the alternate values of the coefficients shown in figures 9 and 10 at the same Mach number and enthalpy are obtained, in better agreement with the higher speed data.

Nose region.- The important change in wave coefficients in the nose regions of these very blunt bodies is shown in figure 11. The change in k is not too great (compare with the curves for $x/d > 2$ brought forward from figure 10), but the exponent n goes down with increasing total enthalpy as the bow wave conforms increasingly to the shape of the nose. Values approaching 0.3 are obtained at the highest test speeds. It is interesting, however, that over the test range, the ratio of nose-region exponent to downstream exponent remains relatively constant, decreasing only a little with increasing total enthalpy. This is shown in figure 12, where the ratio of exponents for the nose and downstream regions is plotted against the nose fineness ratio. (On the abscissa, zero represents the flat face, and 0.5, the hemisphere.) This presentation correlates the nose-region exponents reasonably well. The greatest scatter occurs in the case of the hemisphere, but, as noted earlier, the nose-region data for the hemisphere exhibit appreciable scatter due to measurement errors.

The stations of transition from nose region to downstream region, given in the lower part of figure 11, are generally between 1 and 2 diameters from the wave apex, and show relatively little variation with total enthalpy. In fact, the variation is within the scatter.

Round-Nosed Cones

The downstream wave constants for the round-nosed cones are plotted against total enthalpy in figure 13, and compared with curves brought forward from figure 10. The values of k for these bodies are lower than those for the hemisphere, which is qualitatively consistent with the lower drag coefficients of the round-nosed cones. (See table I and fig. 10.) However, the exponents, n, for the round-nosed cones do not correlate very well with those of the blunter bodies. In some cases, this may be due to the fact that the wave profile data did not extend far enough downstream to define properly the downstream wave equation (see, e.g., upper curve, fig. 4). However, the cone bow waves are less smooth in the

nose region than those of the other bodies, exhibiting abrupt changes in curvature due to strong localized expansions, and so forth, and these disturbances require some distance downstream to become distributed. This might be expected to result in the poorer correlation shown.

The nose-region waves of the round-nosed cones can be approximately described on the basis of some empirical observations. The beginning section of the wave is generated by the spherical nose, and can be computed with the aid of figure 7. (Note that d in equation (2) must for this purpose, be the diameter of the spherical tip.) When the sphere wave becomes approximately parallel to the conical surface, a straight (conical) section of the wave begins. For cone half-angles around 30°, the wave angle in this region is about 1/2 degree greater than the cone angle. For noses of about the proportions shown at the right in figure 1, the straight section can be assumed to run to the model base. However, if the nose radius is small, so that the cone runs back a considerable distance behind the spherical tip, the wave must curve outward to approach the wave angle that would be associated with the pointed cone. These considerations plus a little engineering judgment can lead to a fairly good estimate of the nose-region wave profile.

A 3 6 1

Variations in the Coefficient k With Drag Coefficient

The blast-wave theory predicts that the coefficient k is proportional to the one-fourth root of the drag coefficient (eq. (1)). The extent to which the present data for the downstream region of the waves conform to this will now be considered. If it is assumed that

$$k = aC_D^{\,m} \tag{4}$$

then

$$k_{hs} = aC_{D_{hs}}^{\,m} \tag{5}$$

and, if a is independent of nose shape,

$$\frac{k}{k_{hs}} = \left(\frac{C_D}{C_{D_{hs}}}\right)^m \tag{6}$$

The data on k have been plotted in the ratio form of equation (6) on logarithmic paper in figure 14. This presentation, under the assumption of equation (4), would lead to a straight line plot for all the bodies tested.

For the bodies blunter than hemispheres, $C_D > C_{D_{hs}}$, this is the case. A single line can represent the data with small scatter. The slope of the

line, 0.26, confirms the blast-wave theoretical prediction. The lower drag configurations in this figure are round-nosed cones, and again do not correlate precisely with the other data. However, they disagree by less than 10 percent, and as such, may be said to agree with the theory.

The coefficient a in equation (4) takes values higher than the 0.80 given by the theory, between 1.01 and 1.04 for hemispheres and blunter noses in the present test range, but decreases slowly with increasing total enthalpy. For the round-nosed cones, if m is assumed to be 1/4, 0.95 is a better value for a.

A summary equation for the downstream regions of the waves may be written

$$r_s/d = 1.03\ C_D^{1/4}(x/d)^{n(h_S)} \qquad (7)$$

where the function $n(h_S)$ is given graphically in figure 10. The generality of equation (7) could be improved by replacing the constant 1.03 by a suitable, slowly-varying, second function of h_S which the present data do not adequately define. Equation (7) is recommended for noses blunter than hemispheres.

CONCLUDING REMARKS

These studies show that the various sections of bow-wave profiles generated at hypersonic speeds by blunt-nose bodies can most often be represented by power-law equations. One case has been found, the hemisphere cylinder, in which a single power-law equation describes the entire profile back to where the Mach angle limitation begins to influence the wave. Other cases of this kind may be found; for example, ellipsoidal noses of fineness ratio near 0.5 might have this characteristic. Noses appreciably blunter than hemispheres have wave profiles representable by two power-law equations, one for the nose region and one for the downstream region.

The coefficient and exponent in the power-law equation for the downstream section of the wave can be correlated as functions of total enthalpy, when the Mach number is hypersonic. A single functional dependence of the exponent on total enthalpy was found to apply to four of the seven bodies studied, the hemisphere and the three noses blunter than hemispheres. The constant of proportionality was, for these cases, proportional to the fourth root of drag coefficient, as predicted by blast-wave theory. For the nose region, correlation curves for the coefficient and the exponent were obtained for each nose shape in terms of total enthalpy. It was noted that the nose-region exponent is nearly a fixed fraction of the downstream exponent for each of the blunter-than-hemispherical noses, and that this fraction depends on the fineness ratio of the nose.

While the bow waves of round-nosed cones were less regular in their behavior than the other bodies studied, certain observations concerning these waves also were made, which should provide a basis for first approximations of their profiles.

Ames Research Center
National Aeronautics and Space Administration
Moffett Field, Calif., Sept. 27, 1961

REFERENCES

1. Seiff, Alvin, and Whiting, Ellis E.: Calculation of Flow Fields From Bow-Wave Profiles for the Downstream Region of Blunt-Nosed Circular Cylinders in Axial Hypersonic Flow. NASA TN D-1147, 1961.

2. Lin, S. C.: Cylindrical Shock Waves Produced by Instantaneous Energy Release. Jour. Appl. Phys., vol. 25, no. 1, Jan. 1954, pp. 54-57.

3. Vas, I. E., Bogdonoff, S. M., and Hammitt, A. G.: An Experimental Investigation of the Flow Over Simple Two-Dimensional and Axial Symmetric Bodies at Hypersonic Speeds. Rep. no. 382 (WADC TN 57-246) Dept. of Aero. Eng., Princeton Univ., June 1957.

4. Seiff, Alvin, and Whiting, Ellis E.: The Effect of the Bow Shock Wave on the Stability of Blunt-Nosed Slender Bodies. NASA TM X-377, 1960.

5. Van Hise, Vernon: Analytic Study of Induced Pressure on Long Bodies of Revolution With Varying Nose Bluntness at Hypersonic Speeds. NASA TR R-78, 1960.

6. Seiff, Alvin, Sommer, Simon C., and Canning, Thomas N.: Some Experiments at High Supersonic Speeds on the Aerodynamic and Boundary-Layer Transition Characteristics of High-Drag Bodies of Revolution. NACA RM A56I05, 1957.

7. Seiff, Alvin, and Sommer, Simon C.: An Investigation of Some Effects of Mach Number and Air Temperature on the Hypersonic Flow Over a Blunt Body. NASA MEMO 10-9-58A, 1959.

8. Seiff, Alvin: The Use of Gun-Launched Models for Experimental Research at Hypersonic Speeds. AGARD Rep. 138, July 1957.

9. Carros, Robert J.: Free-Flight Investigation of Static Stability and Drag of Models of the Second and Third Stages of the Hemisphere-Nosed X-17 at Mach Numbers From 4 to 10. NASA TM X-158, 1960.

10. Whiting, Ellis E., and Carros, Robert J.: Free-Flight Investigation of the Static Stability and Aerodynamic Drag of Three Blunt-Nosed Cylinder-Flare Test Bodies at Mach Numbers From 13 to 17. NASA TM X-500, 1961.

11. Gravalos, F. G., Edelfelt, I. H., and Emmons, H. W.: The Supersonic Flow About a Blunt Body of Revolution for Gases at Chemical Equilibrium. Proc. IX International Astronautical Congress, Amsterdam, Aug. 25-30, 1958, vol. 1, pp. 312-332.

12. Feldman, Saul: A Numerical Comparison Between Exact and Approximate Theories of Hypersonic Inviscid Flow Past Slender Blunt-Nosed Bodies. AVCO-Everett Res. Lab., AVCO Corp. Res. Rep. 71, June 1959.

TABLE I.- SHOCK-WAVE DATA AND TEST CONDITIONS

Model diam., in.	M_∞	h_S, Btu/lb	T_∞, °R	$\rho_\infty \times 10^4$, slug/ft³	C_D	k_1	n_1	k_2	n_2	Measurement region x/d min	Measurement region x/d max
Hemisphere cylinder											
0.2137	3.40	421	530	22.70	0.94			1.26	0.543	0.15	4.00
1.903	3.80	486	530	22.70	↓	1.24	0.516			.012	.09
.2137	9.85	908	190	9.35	↓			1.04	.460	.30	8.00
.750	11.60	1246	192	9.88	↓	1.02	.463			.03	.27
.750	11.92	1306	193	9.63	↓	1.13	.503	1.01	.444	.10	3.00
1.159	14.00	1795	190	8.73	↓	1.05	.487	.98	.451	.04	4.00
.200	14.34	1878	188	9.18	↓	[illegible]	[illegible]	1.00	.449	.20	2.50
Theory	18.03	6224	390	2.25	↓			.937	.480	.50	25.00
↓	18.10	8114	509	.01412	↓			.90	.446	.90	5.00
↓	18.24	8112	500	.03564	↓			.91	.454	1.00	5.00
↓	19.25	8103	449	.006118	↓			.89	.442	2.00	5.00
1.200	7.64	564	189	10.11	↓	1.04	.467	1.03	.453	.06	2.09
1.600	8.20	991	300	12.00	↓	1.07	.481	1.04	.464	.10	.50
1.184	9.34	821	191	8.82	↓	1.20/1.11	.524/.494	1.03	.453	.30	1.30
1.159	14.00	1795	190	8.73	↓			.98	.436	.20	1.50
1/7-power nose											
1.200	3.48	399	520	23.62	.95	1.26	.446	1.24	.541	.04	2.7
1.1983	7.59	875	291	18.27	1.02	1.09	.394	1.06	.471	.08	3.1
1.200	7.68	1494	536	22.65	1.05	1.07	.383	1.06	.454	.03	2.5
1.200	10.10	1514	295	12.67	1.07	1.08	.380	1.06	.447	.08	2.6
1.200	10.34	1514	295	12.67	1.07	1.04	.389	1.03	.439	.10	2.0
1.200	14.50	1737	191	8.86	1.10	1.07	.365	1.04	.435	.10	3.0
Flat-faced cylinder											
.5092	4.50	680	527	23.20	1.65	1.40	.411	1.35	.474	.10	4.0
.5092	4.50	680	527	23.20	1.65			1.17	.576	4.00	7.00
.5220	9.29	859	188	9.68	1.70	1.28	.356	1.21	.446	.10	8.0
.5202	10.21	937	188	9.54	1.70	1.29	.357	1.23	.436	.10	9.0
.5094	14.08	1858	192	9.36	1.70	1.26	.326	1.16	.445	.14	9.0
.5094	14.30	1930	192	9.36	1.70	1.22	.314	1.16	.445	.20	9.0
Convex spherical segment (R = d)											
.450	14.25	1890	189	8.64	1.57	1.22	.383	1.12	.452	.11	9.0

Round-nosed cones

Model diam., in.	θ, deg	$\frac{d_t}{d}$	M_∞	h_S, Btu/lb	T_∞, °R	$\rho_\infty \times 10^4$ slug/ft³	C_D	k_1	n_1	$k_{transition}$	$n_{transition}$	k_2	n_2
1.725	30	0.333	8.3	1029	390	17.40	0.54	0.550	0.430	0.780	0.789	0.810	0.554
1.196	30	.333	16.03	2354	187	8.97	.52	.540	.455	.740	.786	.820	.479
1.196	30	.333	16.12	2374	187	8.97	.52	.533	.432	.740	.786	.800	.484
.2800	30	.716	15.05	2075	189	9.186	.682			.865	.570	.875	.455
.2587	22.5	.596	14.9	2035	195	15.15	.478					.795	.526

BLANK PAGE

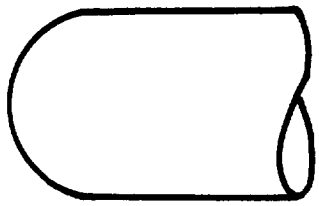

Hemisphere

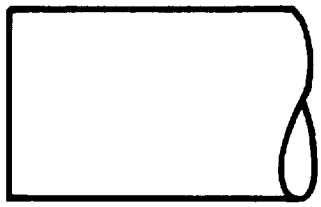

Flat-faced cylinder

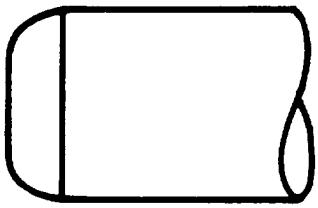

$\frac{1}{7}$ Power nose

$$\frac{r}{d} = \frac{1}{2}\left(\frac{x}{0.3d}\right)^{\frac{1}{7}} = .5939\left(\frac{x}{d}\right)^{\frac{1}{7}}$$

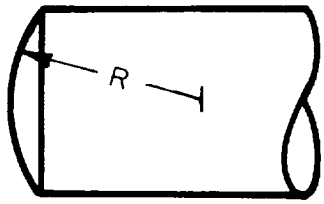

Convex spherical segment, R=d

Round-nosed cones

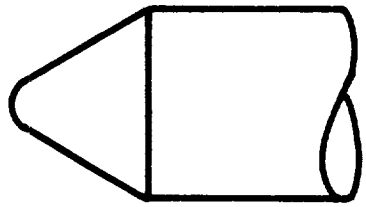

$\theta = 30°,\ \frac{d_t}{d} = 0.333$

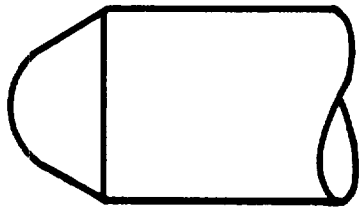

$\theta = 30°,\ \frac{d_t}{d} = 0.716$

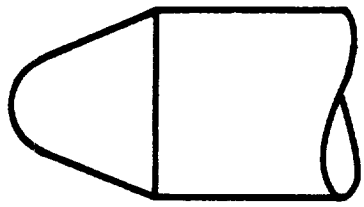

$\theta = 22.5°,\ \frac{d_t}{d} = 0.596$

Figure 1.- Nose shapes included in study.

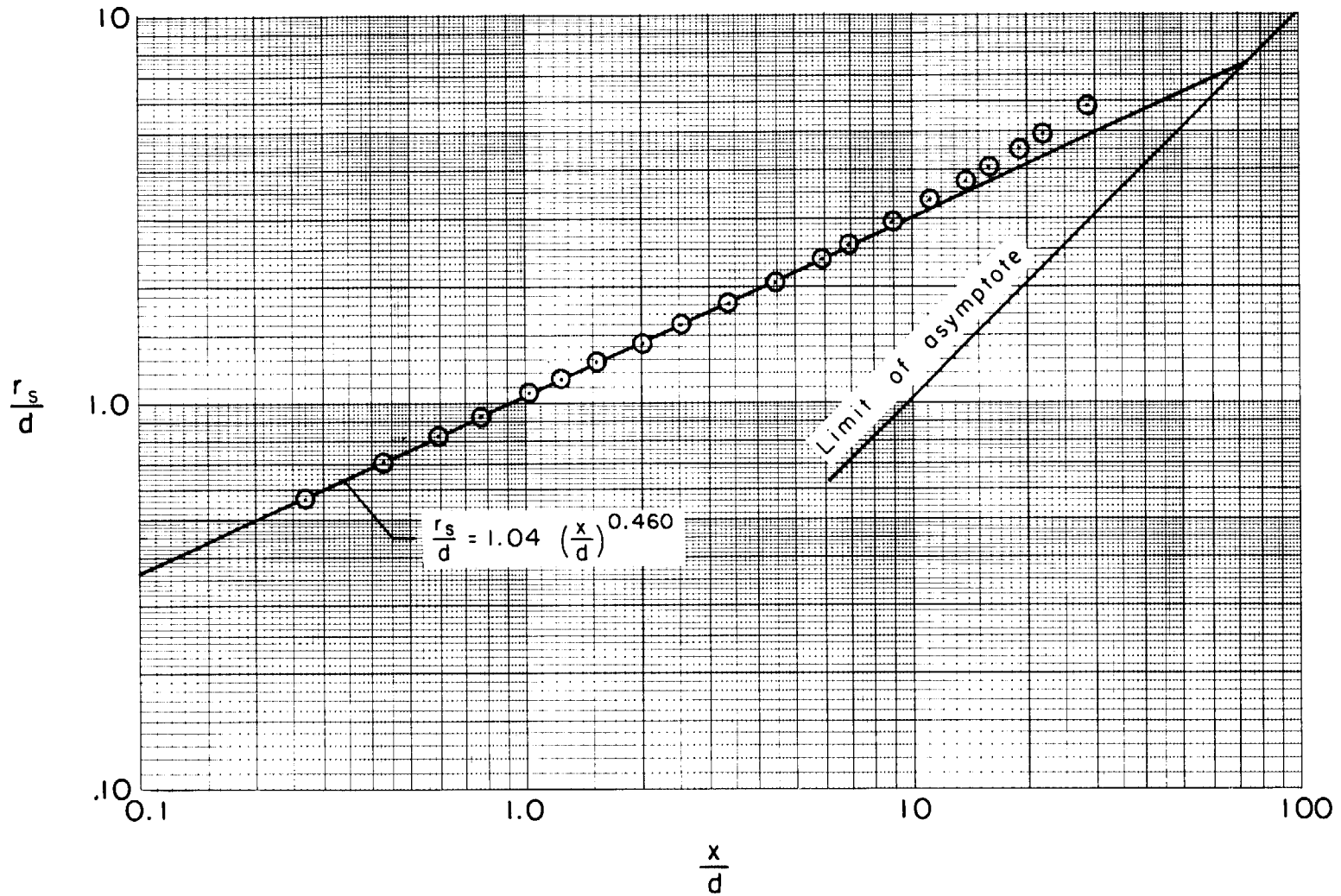

(a) Hemisphere-cylinder. $M_\infty = 9.85$. $h_S = 908$ Btu/lb.

Figure 2.- Logarithmic plots of bow-wave profiles for a hemispherical nose.

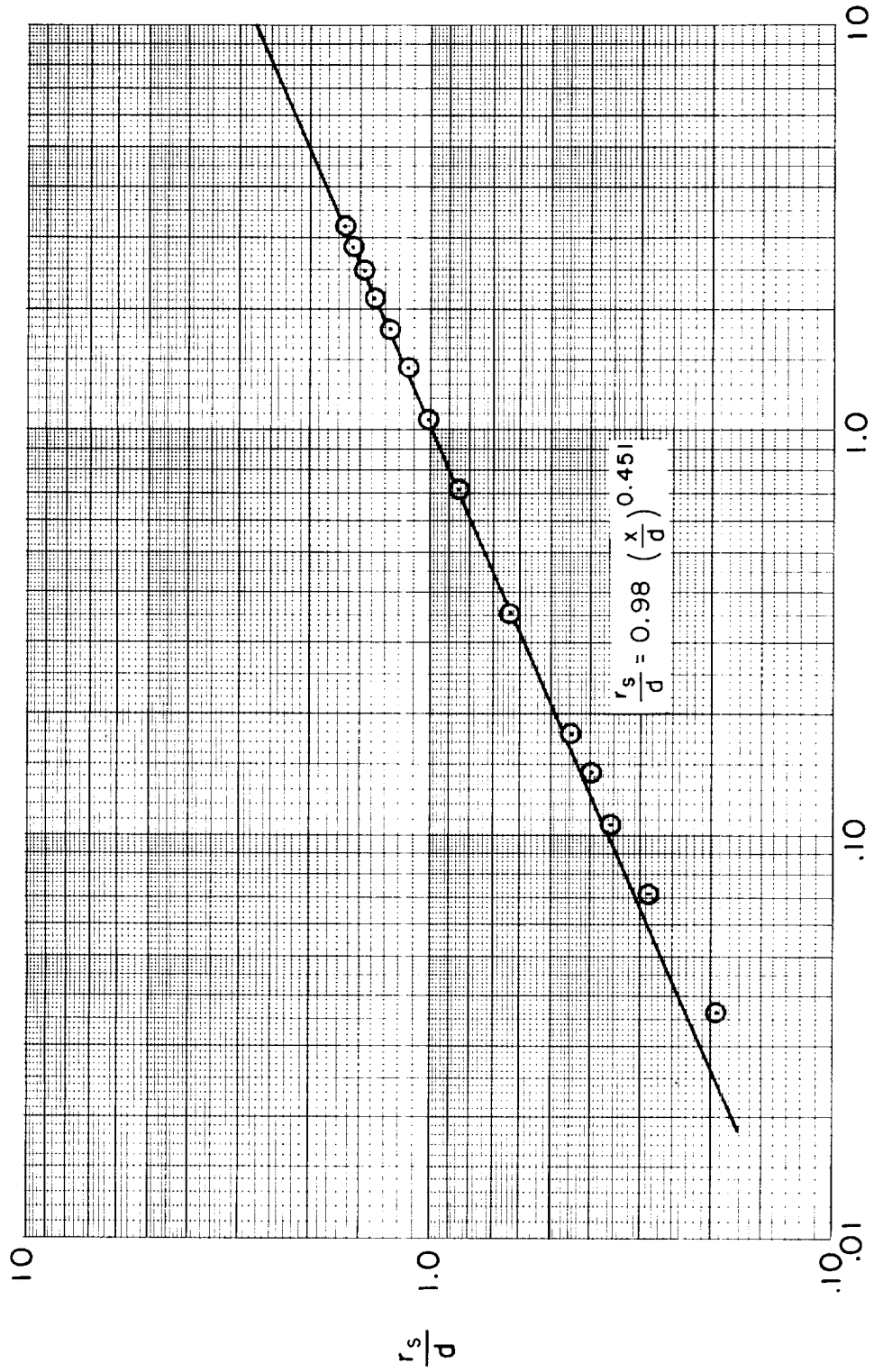

(b) Hemisphere. $M_\infty = 14.0$, $h_S = 1795$ Btu/lb.

Figure 2.- Concluded.

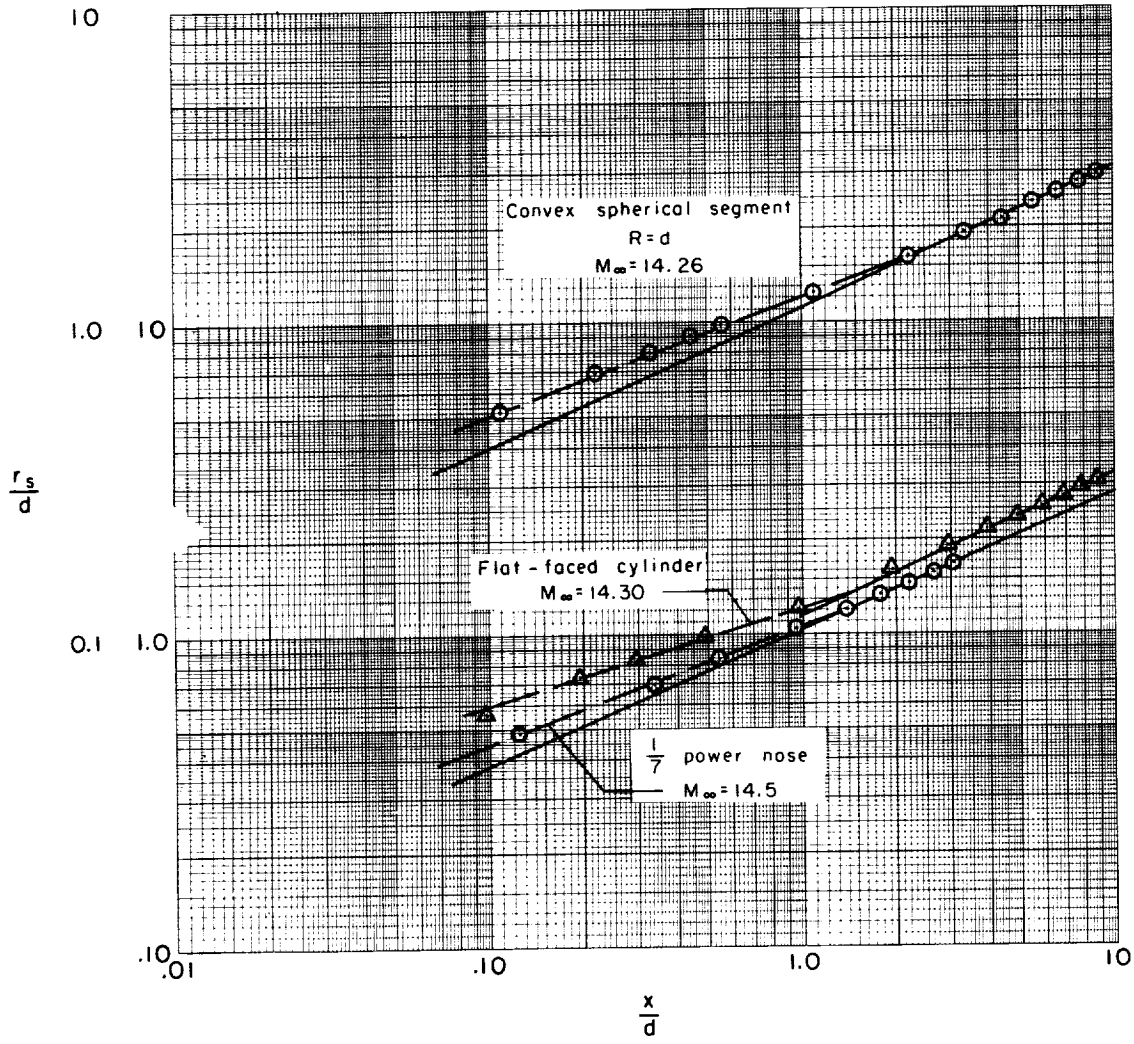

Figure 3.- Logarithmic plots of bow waves from bodies blunter than hemispheres.

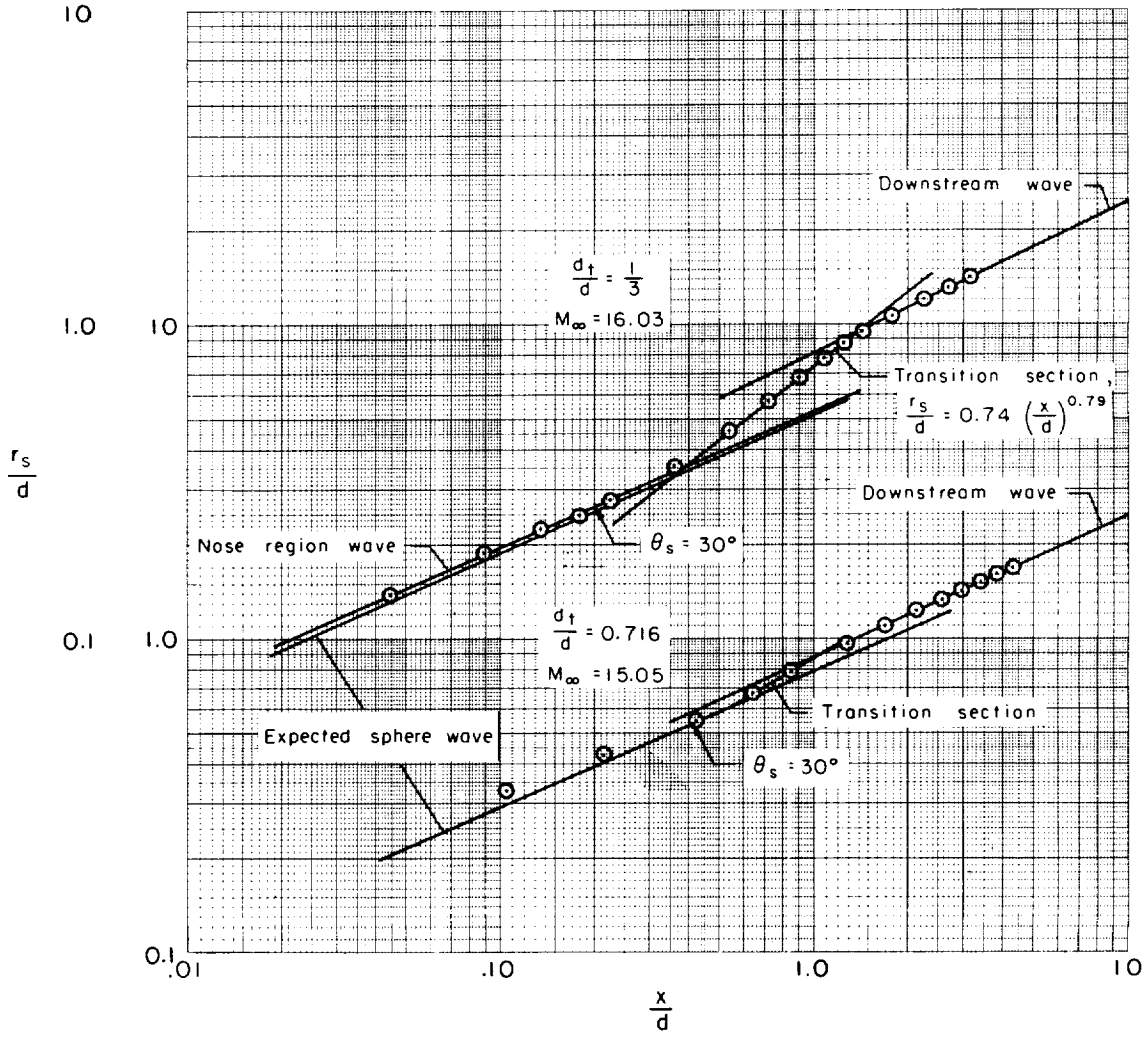

Figure 4.- Logarithmic plot of bow-wave profiles for 30° half-angle round-nosed cones.

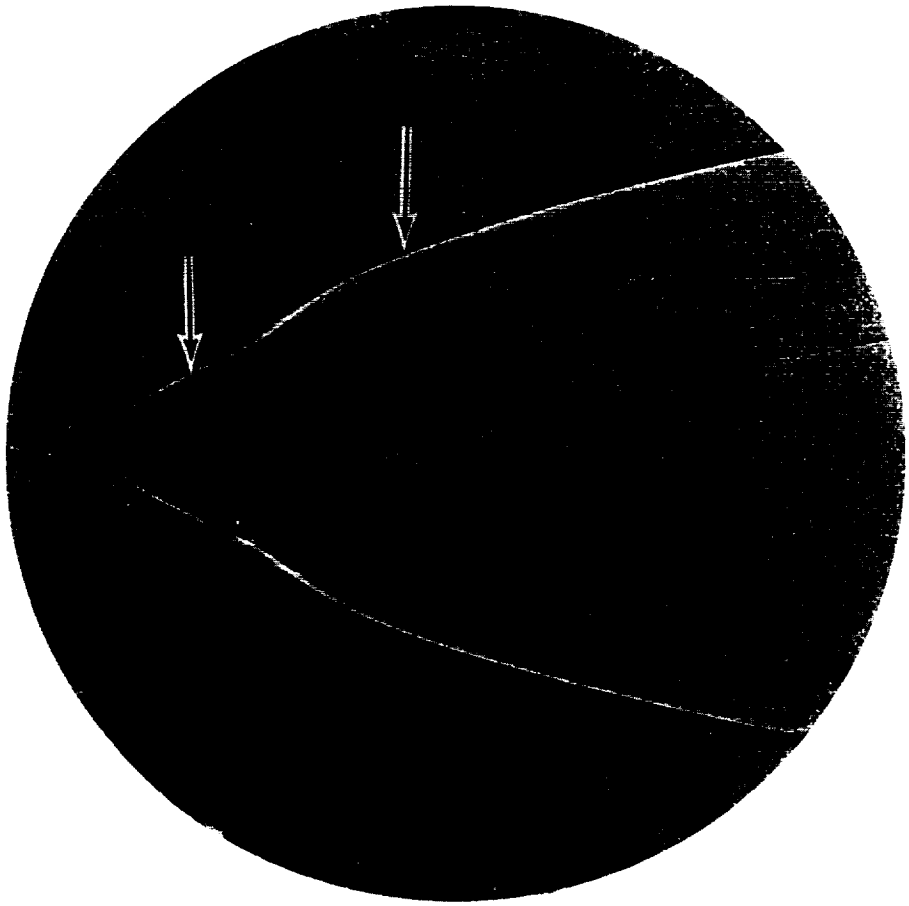

Figure 5.- Shadowgraph of round-nosed cone of 30° half-angle and $d_t/d = 0.333$ at a Mach number of 16.0.

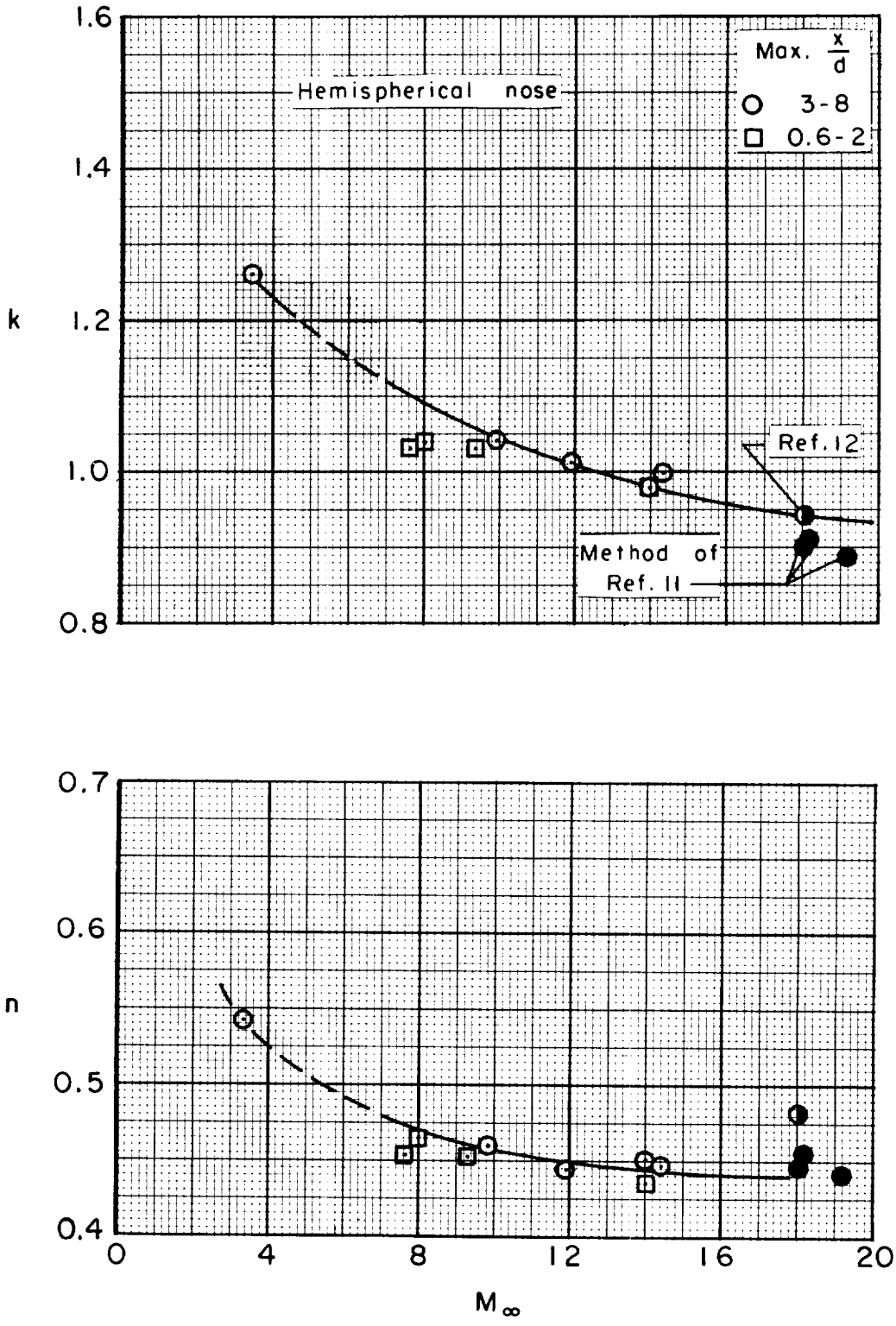

Figure 6.- Dependence of shock-wave constants on free-stream Mach number.

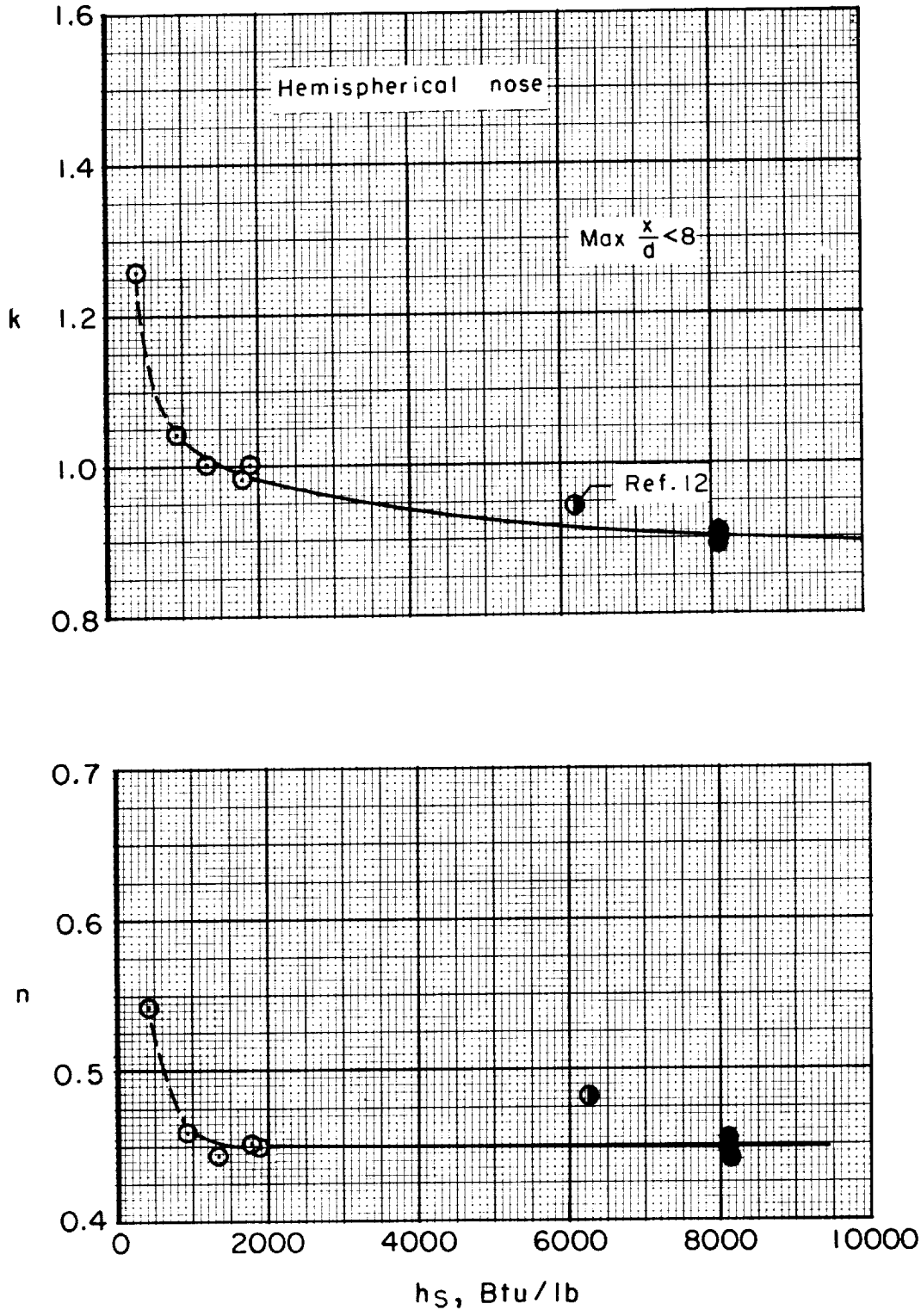

Figure 7.- Dependence of shock-wave constants on total enthalpy.

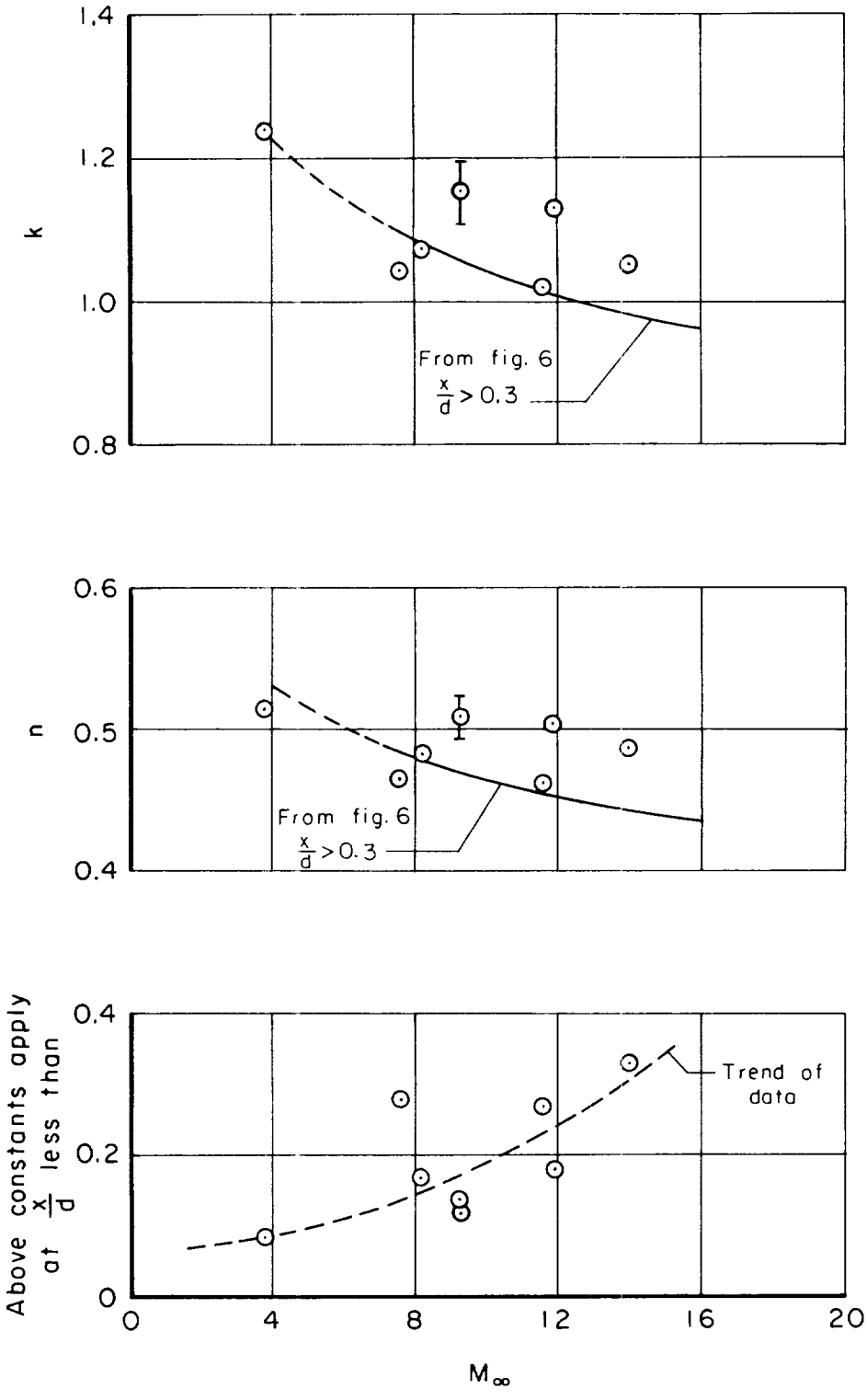

Figure 8.- Bow-wave constants for region very close to hemispherical nose.

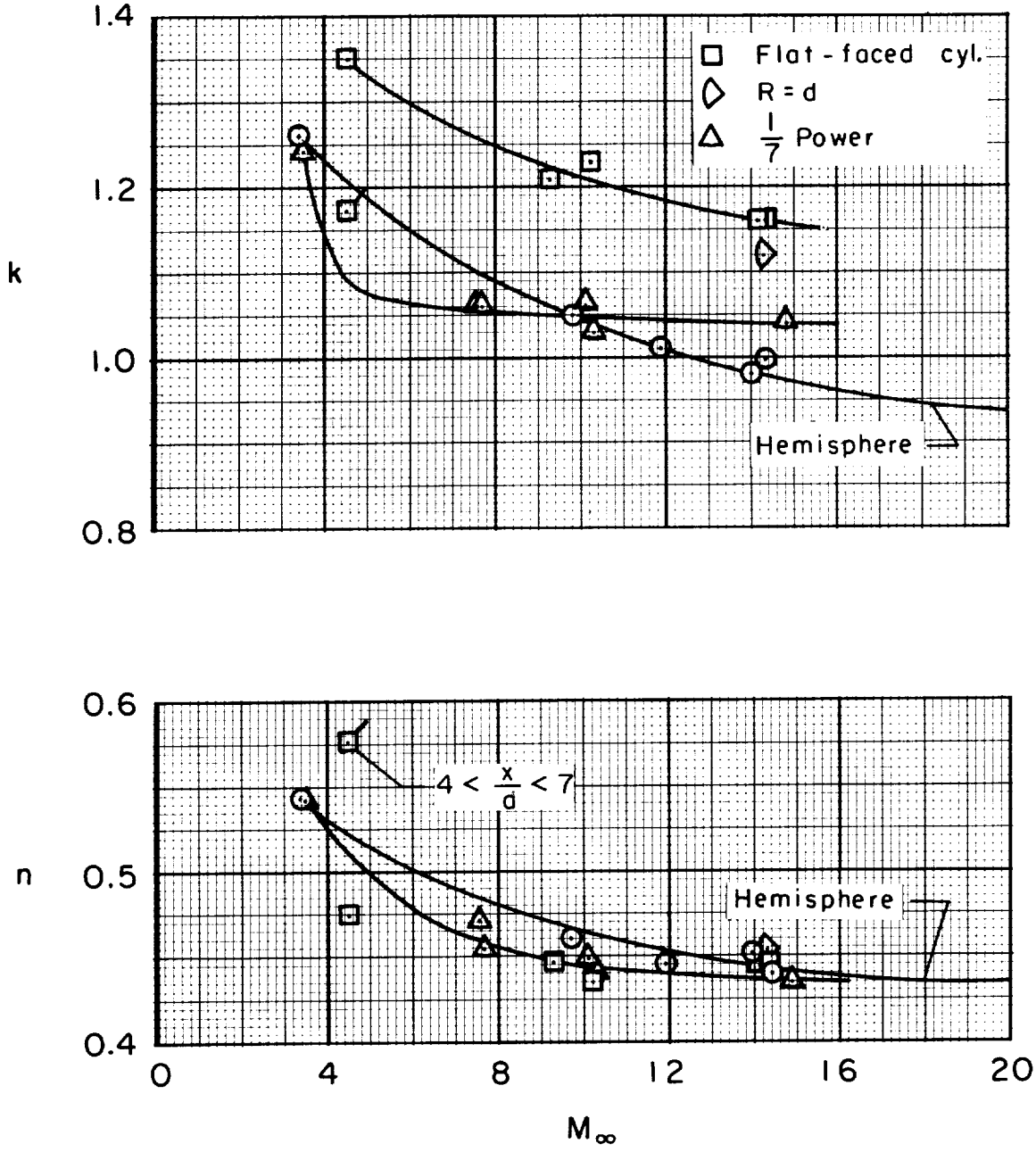

Figure 9.- Downstream wave constants as function of Mach number for noses blunter than a hemisphere.

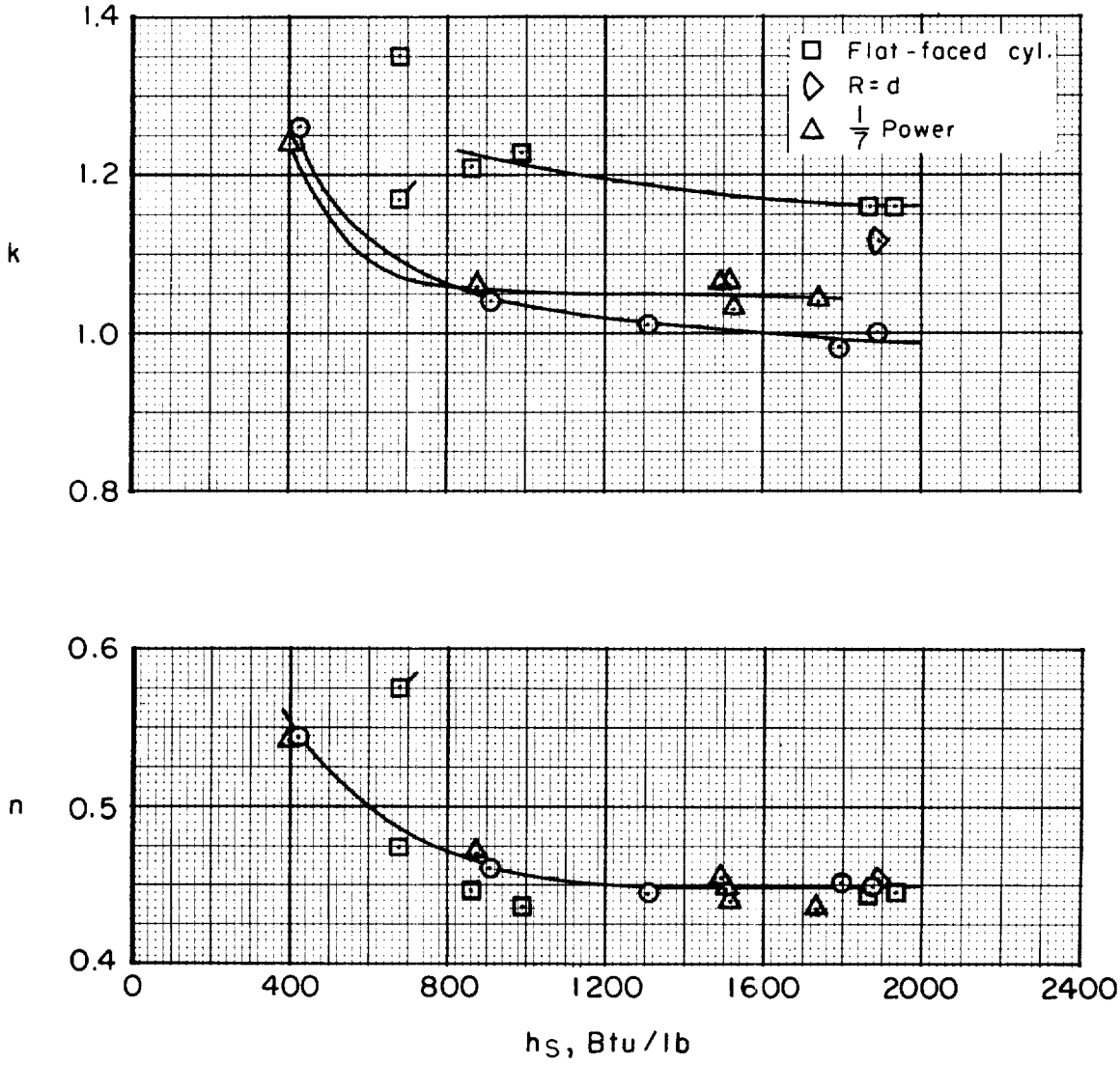

Figure 10.- Downstream wave constants as function of total enthalpy for noses blunter than a hemisphere.

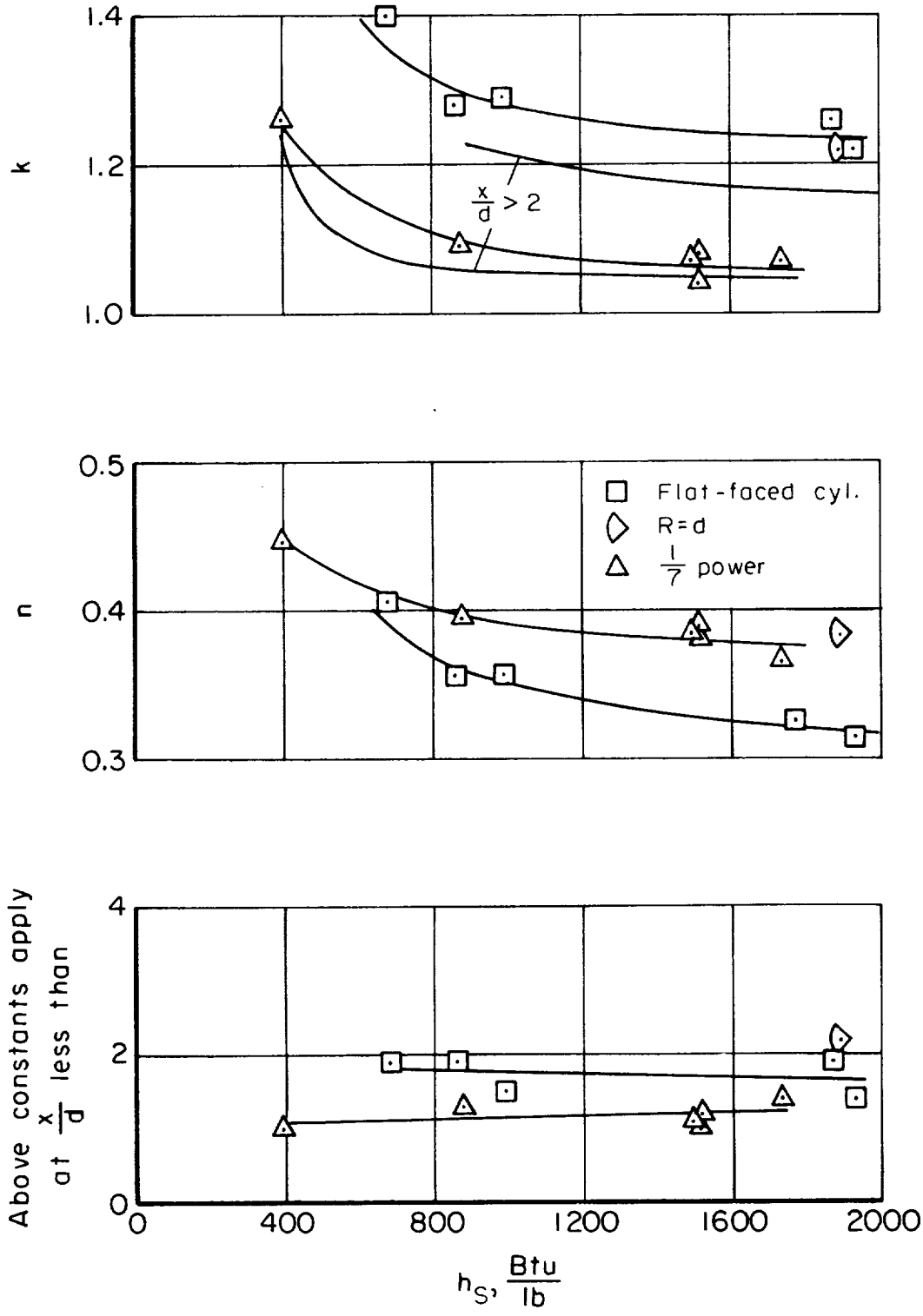

Figure 11.- Nose-region wave constants for noses blunter than a hemisphere.

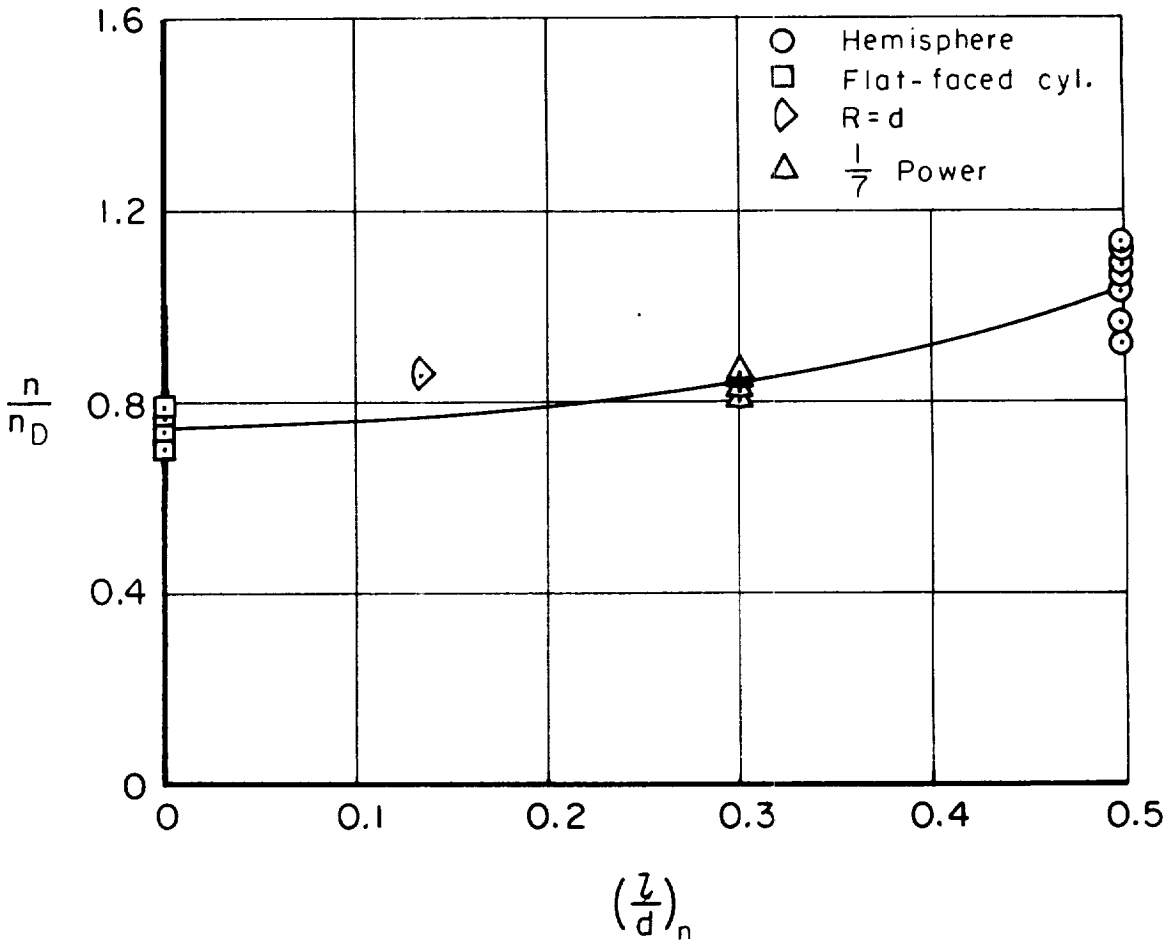

Figure 12.- Correlation of nose-region exponents for noses blunter than hemispheres on the basis of nose fineness ratio.

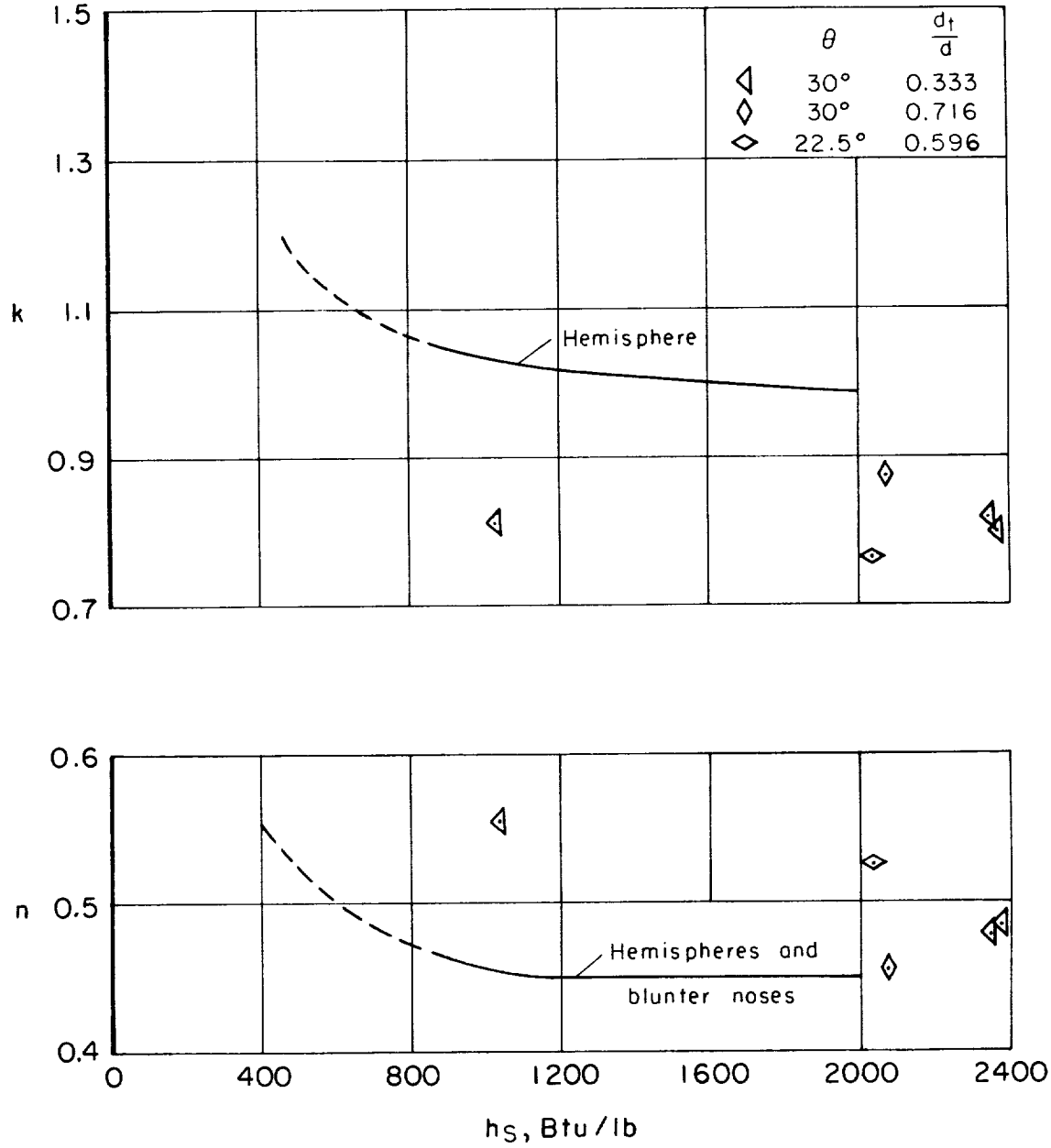

Figure 13.- Downstream wave constants for round-nosed cones.

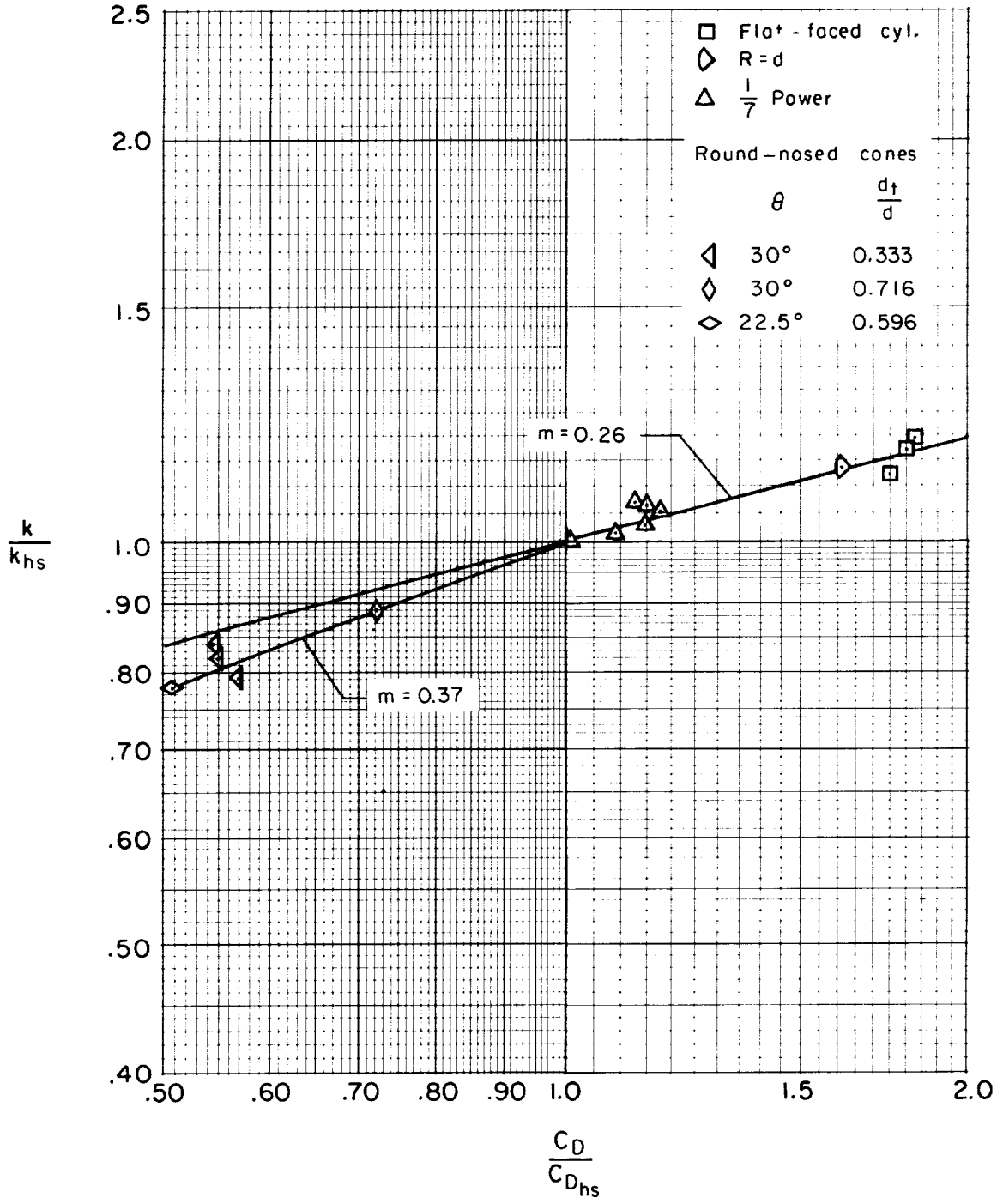

Figure 14.- Correlation of constants k on basis of nose drag coefficient.